Bitlis Eren Üniversitesi Fen Bilimleri Dergisi
BİTLİS EREN UNIVERSITY JOURNAL OF SCIENCE
ISSN: 2147-3129/e-ISSN: 2147-3188
VOLUME: 11 NO: 3 PAGE: 902-910 YEAR: 2022
DOI: 10.17798/bitlisfen.1139679

Residual Stress Measurement of a Single-step Sintered Planar Anode Supported SC-SOFC Using Fluorescence Spectroscopy

Yunus SAYAN[1,2*], Jung-Sik KİM[2], Houzheng WU[2]

[1] *Bitlis Eren University, Faculty of Engineering and Architecture, Department of Mechanical Engineering, Bitlis, Türkiye*
[2]*Loughborough University, School of Aeronautical, Automotive, Chemical and Material Engineering Loughborough, United Kingdom*
(ORCID: 0000-0002-0871-6842) (ORCID: 0000-0002-3696-7251) (ORCID: 0000-0002-7628-3890)

Keywords: Residual Stress, Fluorescence Spectroscopy, Sintering, Solid Oxide Fuel Cell.

Abstract
The fluorescence spectroscopy technique was used to measure the residual stress between the cathode and electrolyte of an anode supported planar single-chamber solid oxide fuel cell. The cell was made of (NiO-CGO): (CGO): (LSCF-CGO), as anode:electrolyte:cathode and the test was carried out after sintering at room temperature. The measured stress between these layers arises from the sintering stress caused by differential shrinkage from layers during sintering and the thermal expansion co-efficient mismatch between the layers during cooling. Therefore, the residual stress in the cathode and electrolyte layer of the cell due to co-efficient of thermal expansion mismatch during cooling was calculated analytically so as to find sintering stress. According to findings a maximum compressive residual stress of -1084 MPa occurred at the place contiguous to electrolyte layer. The estimated residual stresses in the cell's cathode and electrolyte layer owing to CTE mismatch for the duration of cooling was calculated as -324 MPa and 15.96 MPa, respectfully. Furthermore, total mean residual compressive stress between cathode and electrolyte was obtained from fluorescence spectroscopy as -703.795. Thus, the main contribution of this residual stress is the stress growth during sintering (-395.755 MPa) due to different shrinkage behavior of adjacent layers.

1. **Introduction**

The composites of multi-layered ceramic may undergo substantial magnitude of residual stress during cooling from sintering temperature. Residual stress particularly occurs when they are comprised of considerably thick layers made of different laminations or materials. In addition, different co-efficient of thermal expansion (CTE) between layers and elastic constants among neighboring layers and between the component phases are the main cause of the residual stress [1], [2]. Furthermore, the resistance of a cell to residual stress-induced cracking or deformation is significantly affected by the layered structure's geometry on layer thickness. The general stress area may be quite complex and thus difficult to predict by theoretical calculations. In order to avoid cracking and delamination, a precise control of both distribution and magnitude of residual stress is needed. To assess the residual stress in the components of multi-layered ceramic, a development of reliable experimental method is substantially desired. X-ray diffraction, neutron diffraction and piezo-spectroscopic analysis of photo-stimulated fluorescence are some techniques existed to evaluate the residual stress in ceramic materials [1], [3].

In the present study, residual stress between electrolyte and cathode of an anode supported planar single chamber solid oxide fuel cell (SC-SOFC) was measured by the fluorescence spectroscopy technique. This technique can be applied to the materials which must have the luminescent ability. Luminescent material contains $Al_2O_3:Cr^{3+}$, $BaSO_4$, end so on.; for more information about luminescence

*Corresponding author: ysayan@beu.edu.tr
Received: 02.07.2022, Accepted: 23.09.2022

materials can be found in references [4], [5]. In addition, in order to stimulate luminescence, an energy source is required. There are an extensive range of energy sources that can be used, as, UV emission of a gas discharge, cathode rays, X rays, etc., and their variation offers an appropriate classification for luminescence phenomena [4], [5].

It is common knowledge that vast majority of ceramics are optically transparent, aside from pore scattering and grain boundary, because of their large band gabs. Nevertheless, when the existence of trace impurities in polycrystalline ceramics, mostly transition-metal ions and rare-earth ions, are suitably excited, they can generate intense fluorescence. These specific lines usually originate from electronic transition of dopant ions and, moreover, they are excessively sensitive to the local ionic surroundings in the host crystal. Therefore, distortion which alters the interionic distances can bring about change in the characteristic lines. Furthermore, the present degeneracy of the energy states is eliminated by that distortion which reduces the crystal's symmetry, and consequently leads to splitting and shifting of the lines in the spectra. The link amongst the change in energy of the electronic state and strain (equally stress) is defined as the piezo spectroscopic effect [6], [7].

Al_2O_3:Cr^{3+} polycrystalline ceramics powders are chosen to be utilized between the electrolyte (CGO) and cathode (LSCF-CGO) of the cell because they both do not possess luminescent ability. Al_2O_3 corundum are preferably selected by reason of the fact that (1) its sintering temperature is above 1400˚C as per CGO [8]; (2) it has decent chemical and thermal stability, and moderately good strength [9]; (3) it can increase the electrolyte (CGO) ionic conductivity [10], [11]; (4)) it is inactive toward electrolyte material at 1200˚ [11], [12]. However, utilizing alumina powder between these layers to measure the stress may have adverse or beneficial effect on the cell sinterability in addition to cathode electrical and catalytic properties. These effects are not examined and ignored in this study.

The residual stress for alumina-based ceramics can be investigated by Chromium ions (Cr^{+3}) fluorescence spectroscopy method. This technique utilizes the shift in fluorescence bands. These bands are related to Cr which is persistent impurities in Al_2O_3 (alumina) [6], [7], [13], [14]. The oxygen ions' octahedral arrangement surrounding the chromium ions in alumina results in a crystal field and this brings about two closely-separated R1 and R2 bands that fluoresce at a wavelength of nearly 694 nm [14], [15]. Different composition of chromium, temperature change and stress application all distort octahedral and associated crystal field and leads to alterations in the energies of the R1 and R2 fluorescence peaks. This technique basically explained by Huang et al. as a laser being focused on the surface of the sample by using an optical microprobe. The laser interacts with chromium ions in alumina and results in luminescence. Once the materials subject to a stress the luminescence frequency peaks in the spectrum varies accordingly. This fact aids one to acquire the measurement of the mean stress distribution in materials [13]. When the materials undergo tensile stress, fluorescence spectra changes towards higher wavenumber, and vice versa when they undergo compressive stress [16]. Following base equation (Equation 1) gives the connection between stress, σ, and energy change, Δv, (in wavenumbers, cm^{-1}), in the Al_2O_3 corundum form [3], [6], [7], [14], [15], [17], [18]:

$$\Delta v=\Pi_{11}\sigma_{11}+\Pi_{22}\sigma_{22}+\Pi_{33}\sigma_{33} \quad (1)$$

Where the corundum crystallographic axes (a, m, c) are represented with the tensor axes (1, 2, and 3). The uppercase of Pi (Π) defines the piezo-spectroscopy coefficient. In addition, the threefold rotational symmetry around the corundum c axis should essentially give rise to the m and an axes to be equivalence. For that reason, it is assumed here that conventional notation of Π_{11}, Π_{22}, Π_{33} can be utilized as $\Pi_{11} = \Pi_{22} = \Pi_a$ and $\Pi_{33} = \Pi_b$. Furthermore, these two piezo-spectroscopy coefficients (Π_a and Π_b) are not the same for the fluorescence lines of R1 and R2. Consequently, under the hydrostatic conditions, ($\sigma_{11}= \sigma_{22} = \sigma_{33} = \sigma$), the above base equation (Equation 1) can be rearranged as follows [14], [15]:

$$\Delta v=(2\Pi_a+\Pi_b)\,\sigma \quad (2)$$

Though the Π_a and Π_b, for R1 and R2 fluorescence lines, respectively, are different [6], [14], [19], the pressure sensitivity of them ($2\Pi_a + \Pi_b$) is approximately the same [20]–[22]. To calculate residual stress between the cathode and electrolyte of the cell, R1 line shifts will here be of interest. The piezo-spectroscopic coefficient for R1 line can be calculated from the definition given in the following parenthesis (2/3 of ($2\Pi_a + \Pi_b$)) for polycrystalline A_2O_3 and as a result, it can be found as $(7.59 \times 2) / 3 = 5.06$ cm^{-1} GPa^{-1} [3], [6].

Furthermore, residual stress in the sintered cell is caused by (1) stress growth during sintering owing to different shrinkage rate of layers and (2) thermal expansion misfit of layers while cooling from 1200˚C to 20˚C. When the sintered cell's residual stress at 20˚C (assumed to be room

temperature) because of different thermal expansion mismatch during cooling is calculated, afterwards the residual stress developed during sintering can be predicted from residual stress measurement at room temperature applying fluorescence spectroscopy technique. Equation 3 can be easily utilized so as to obtain residual stress contribution due to CTE misfit for two different layers. However, the sintered cell consists of three different layers, cathode, electrolyte and anode. Nevertheless, the equation 3 can still be utilized for the cell in this study if one accept electrolyte and anode as one sheet because the anode and electrolyte possess close shrinkage properties [23] and CTE (see Table 1). Besides, the anode itself is composed of 40% of electrolyte (CGO) material before sintering and the electrolyte thickness is relatively small comparing to anode for the anode supported planar SC-SOFC. Therefore, the anode/electrolyte layers can be presumed to be one composite layer containing NiO-CGO materials with certain porosity.

$$\sigma_1 = \frac{(\alpha_2 - \alpha_1)\Delta T}{\frac{1}{\hat{E}_1} + \frac{t_1}{t_2}\frac{1}{\hat{E}_2}} \quad \text{and} \quad \sigma_2 = \frac{(\alpha_1 - \alpha_2)\Delta T}{\frac{1}{\hat{E}_2} + \frac{t_2}{t_1}\frac{1}{\hat{E}_1}} \quad [24] \quad (3)$$

$$\hat{E} = \frac{E}{1-v} \quad [24] \quad (4)$$

$$v = \frac{E}{2G} - 1 \quad [25] \quad (5)$$

Where E is the young`s modulus, v the Poisson ratio, σ the residual stress in layers, α the coefficient of thermal expansion, G the shear modulus, ΔT the change in temperature, and t the layer thickness. Subscripts 1 represents the cathode layer and subscript 2 represents the single composite new layer.

In the present study, the total residual stress after sintering between electrolyte and cathode of an anode supported planar single chamber solid oxide fuel cell (SC-SOFC) caused by sintering stress due to differential shrinkage from layers during sintering and thermal expansion co-efficient mismatch between layers during cooling was measured utilizing fluorescence spectroscopy at room temperature (20ºC). In addition, equation 2, 4 and 5 were used to calculate analytically the residual stress in cathode layer of the cell owing to CTE misfit during cooling at 20ºC. By subtracting the calculated residual stress from total residual stress, the sintering residual stress contribution was estimated.

2. Experimental

2.1. Row Materials

The cell was comprised of (NiO-CGO): (CGO): (LSCF-CGO), as anode:electrolyte:cathode materials (A:E:C). Green layers were made via tape-casting process and composed of 60 wt% NiO–40 wt% $Ce_{0.8}Gd_{0.2}O_{2-\delta}$ as anode (NiO-CGO), $Ce_{0.8}Gd_{0.2}O_{2-\delta}$ as electrolyte (CGO) and 50 wt% $La_{0.6}Sr_{0.4}Co_{0.2}Fe_{0.8}O_{3-\delta}$ –50 wt%CGO (20% Gd) as cathode (LSCF-CGO). These layers were purchased from Maryland tape-casting Ltd, USA [26]. In order to obtain the designed thicknesses of the electrolyte and electrodes for the anode-supported planar SC-SOFC, these green layers were stacked and subsequently hot-pressed. Details of the chemicals made the green tapes are given by the supplier, and can be found in reference [23]. In addition, the particle size of the cathode green band was chosen to be 1 µm, as opposed to 0.3 µm for the electrolyte and anode green tapes, so as to retard the sintering of the cathode.

2.2. Cell Preparation

Individual layers of green tape, around a thickness of 20 µm per layer, were stacked sequentially on top each other in accordance with the required thickness of cathode, electrolyte and anode. Alumina fine particles (CTM-DAR. 99.99% purity and possession a mean particle size of 200 nm) were sprinkled carefully for a reasonably homogeneous distribution between electrolyte and cathode during stacking step as presented in Figure 1 so as to make a cell for fluorescence spectroscopy measurement. Thereafter, these stacked layers were hot-pressed at 60 ˚C and 2 MPa with a dwelling time of 5 minutes using Carvel Heated Bench Top Hot Press (model: 3853CE-8, USA) with the purpose of allowing individual layers combined together to form a complete cell. The hot pressed cell then sintered at a temperature of 1200 ˚C for 1 hour. A heating and cooling rate profile during sintering were determined as following: 1˚C min^{-1} heating rate from 20 ˚C to 500 ˚C, a heating rate of 2 ˚C min^{-1} from 500 ˚C to 900 ˚C, 1 ˚C min^{-1} heating rate from 900 ˚C to 1200 ˚C; and 3 ˚C min^{-1} cooling rate from 1200 ˚C to 20 ˚C. As a result, an anode supported SC–SOFC was obtained and possesses the width (W) and length (L) of 40 mm × 40 mm (W × L). Moreover, the anode, electrolyte and cathode of the cell has a thickness of 800:20:40 µm, respectively.

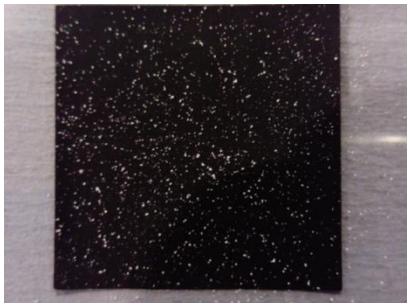

Figure 1. Distribution of sprinkled alumina powder on the surface of stacked cathode layers before stacking electrolyte layers.

2.3. Porosity Measurement

The technique applied to assess the mean porosity of the cathode, electrolyte and anode of the cell can be explained as follows: Back scatter SEM images of cross-sectional areas of the cell layers (anode, cathode and electrolyte), having a Mag 2.00 KX, 10 µm scale and 8.5 mm WD, were taken separately. Thereafter, the obtained SEM images were sent to the ImageJ program and were set to 8-bit image quality in order for threshold analysis. Each images' threshold was adjusted carefully. The percentage of the black regions on the SEM images, corresponding to the percentage of the porous region, were read on the ImageJ program and noted (Table 2).

2.4. The Estimation of the New Values of Young`s Modulus, CTE, and Poisson Ratio

The cell which has the three-layered structure (the cathode, electrolyte and anode) were assumed to be a two-layered structure so as to utilize equation 3. It was supposed that and electrolyte (CGO) and anode (NiO-CGO) as one composite layer because the composite anode comprises of 60% of NiO and 40% of electrolyte (CGO) material before sintering. Furthermore, their shrinkage and CTE properties are close to each other (see Table 1). In addition, the electrolyte thickness is relatively thin compared to the anode for the anode supported planar SC-SOFC. Thereby, anode/electrolyte layers can be assumed to be one layer containing NiO-CGO materials with certain porosity and are defined as a single composite layer. Moreover, the cathode also consists of different composition, 50%LSCF-50%CGO, before sintering, however, the co-efficient of thermal expansion and the shrinkage rate [23] of the CGO electrolyte and cathode are quite different (see Table 1). Therefore, the sintered anode supported planar SC-SOFC can be assumed to has two layers which are designated as a composite cathode layer and a single composite new layer. Additionally, the cell's cathode layer possesses certain porosities after sintering. Thus, the pore percentage and each material composition should be taken into consideration to obtain true value of Poisson ratio, Young`s modulus and thermal expansion coefficient of these materials. The inclusion principle can be easily used in order for finding these values.

Table 1. Estimated properties of some materials from literature with around 99% relative density.

	Material properties		
	CTE (K^{-1})	E (GPa)	v
NiO	13.3 x 10^{-6} [27]	220 [28]	0.31 (calculated from equation 5)
CGO	12.96 x 10^{-6} [24]	200 [24]	0.33 [24]
LSCF	16.12 x 10^{-6} [29]	157 (152 at 95.4 density) [30]	0.3 [30]

Estimated properties of some materials (NiO, CGO and LSCF) with around 99% relative densities used in this study are summarized in Table 1. This information was obtained from literature. The single composite new layer, however, contains CGO, NiO and certain porosities. The sum of the CGO volume in the composite anode and electrolyte gives the CGO volume in the single composite new layer. Likewise, the pores of the electrolyte and composite anode were summed to calculate the single composite new layer's porosity. Considering the NiO, CGO and total porosity of the single composite new layer (see Table 2), the new values of CTE, Poisson ratio, and Young`s modulus of this layer were calculated using the information provided in Table 1 and Table 2 by easily utilizing inclusion principles. Furthermore, the composite cathode is composed of CGO, LSCF and porosity. Therefore, its new properties were calculated based on its composition in the same way as single composite new layer (see Table 2) (each layer's mass ratio in the green tape was presumed to be equal with the volume ratio). In addition, the thickness of cathode and single composite new layer after sintering were calculated according to approximately 18% shrinkage of each layer from SEM results.

Table 2. New material properties calculated based on their composition and porosity ratio using simple inclusion principle

	LSCF %	CGO %	NiO %	Porosity	CTE (K^{-1}) x 10^{-6}	E (GPa)	Ê (GPa)	v	t (μm)
Cathode	37.39	37.39	0	25.22	10.87	133.48	174.6	0.235	32.8
Single composite new layer	0	29	41	30	9.21	148.2	190.7	0.223	672.4

2.5. Fluorescence Spectroscopy for Determination of Residual Stress

Residual stress of Al_2O_3 inclusions between electrolyte and cathode of the cell was measured using Fluorescence spectroscopy. Figure 2 displays an illustrative alumina inclusion sitting in between electrolyte and cathode layers of planar SC-SOFC. Furthermore, mapping on alumina for the measurement points of the fluorescence spectra and its initial point are also shown in the same figure. A step size of 1 μm for a 40 × 9 points on x and y direction, respectively, (mapping of 39 μm × 8 μm) was determined to take measurements. In order to obtain non-distorted and reasonable fluorescence spectra from the points on alumina particles, a representative 9 points on y direction for each 24 points along x direction, out of 40 × 9 points, were chosen for the measurement of the stress, as displayed in Figure 2. Measurements of the fluorescence spectrum were taken on the locations where proper alumina was found for simplicity.

A true confocal Raman microscope (The LabRAM HR High Resolution Raman/PL Microscope system, Horiba, Japan) was utilized to obtain fluorescence spectra from alumina located between electrolyte and cathode layer of the sintered anode supported planar SC-SOFC. Fluorescence spectra were also taken from unstressed alumina which are positioned on the top of the glass plate during measurement for reference spectrum. Each fluorescence spectra were taken over 14268 cm^{-1}–14539 cm^{-1} spectrum with a 633 nm red line of a 17 mW He-Ne laser. In addition, a 50X objective lens in cooperation with a confocal setup which comprised two 50 μm pinhole apertures at 90˚ to one another providing an approximate 1 μm beam diameter on the specimen surface were used to take measurements. Furthermore, the grating of the scanning spectrometry was set to 1800 cm^{-1}.

An interest area for each measurement was selected by using the optical microscope concentrated on the top surface plane of the cell cross-section area where alumina situated and on the top of the unstressed reference alumina powders located on the top of the glass plate by changing of the sample stage height. All experiments (together with calibration) were done in a controlled atmosphere at 22 $\pm$ 2˚C. A step size of 1 μm for a 10 μm × 1 μm for unstressed alumina powders positioned on the glass sheet and a 39 μm × 8 μm mapping for alumina between layers were set to take measurements. In addition, acquiring time was adjusted to 10 seconds for each point. Thereafter, curve-fitting algorithms included in the Origin 2015 software were used to analyze the obtained data. The mean reference spectrum was calculated by averaging the 10 measured strain-free alumina powder spectrum. Moreover, in order to obtain energy change (Δv), the mean R1 fluorescence peak of unstressed alumina was subtracted from R1 fluorescence peak of stressed alumina located between electrolyte and cathode of the cell. Finally, dividing energy change by 5.06 cm^{-1} GPa^{-1} as defined above paragraphs, the total stress at each point was obtained.

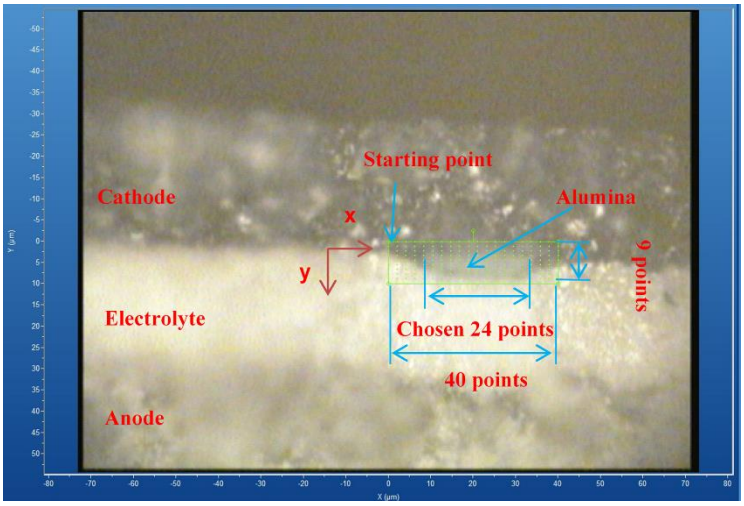

Figure 2. A representative illustration of an alumina particle sitting in between cathode and electrolyte layers of a SC-SOFC and mapping positions on alumina for fluorescence spectrum measurement.

3. Results and Discussion

One of the fluorescence spectra obtained from the cell and the one from reference alumina are shown in Figure 3. The shift ($\Delta\nu$) of peaks, R1 and R2, can be clearly seen on the figure. According to Figure 3 the shift is in the direction of lower wavenumber (from 14404 cm^{-1} to 14398.9 cm^{-1}); demonstrating a compressive stress. All measurements taken from the cell have shift towards lower wavenumber according to acquired results. This shows that all particles of alumina are under compressive stress therein the placed position in the cell after sintering.

The map of the residual stress in a particle positioned between electrolyte and cathode of the anode supported planar SC-SOFC at room temperature are shown in Figure 4. The measured residual stress between the cathode and single composite new layer after sintering originates from different shrinkage behavior of layers during sintering and CTE mismatch of these layers during cooling. Alumina powder existing between layers of the cell may affect the cell sinterability compared to the similar cell sintered without alumina powder. Thus, the residual stress in the actual cell sintered without alumina powders may not be the same with that of the cell sintered with alumina powder. Nevertheless, this effect was neglected as a first approach for the good of quantifying the residual stress in the cell by using fluorescence spectroscopy. Although the actual cell might have different residual stress in comparison to the similar cell that alumina powders were located between layers, using fluorescence spectrum for the cell residual stress measurement can aid one to assess the stress distribution in the cell and therefore gain better knowledge of entire sintering process.

In accordance with Figure 4, a maximum compressive residual stress of -1084 MPa occurred at the place near electrolyte layer. The electrolyte higher densification by comparison cathode (according to the SEM images of past puplication, cathode possess higher porosity than electrolyte) could be the explanation for the residual stress location of the cell, which were detected in the previous study [23]. The higher densification of electrolye maight cause more pressure on alumina section in the electrolyte during sintering. In addition, the main observed point for the cell is the absence of symmetrical residual stress distribution along the x direction from the alumina particles, having an area of relatively higher stress near the x = 0–10 region. This might be explained as the location of the measured alumina particles has not the same equidistant to the edges of the cell. Thus, bending effect owing to the different shrinkage of layers has asymmetrical impacts to the alumina powders. For example, if the powder of the measured alumina is closer to one of the cell edge, the effect of compressive stress will be greater at the alumina edge which is facing the edge of cell far away from it. Furthermore, for each point in the x-direction, the average residual stress throughout the y-direction was also calculated (see Table 3).

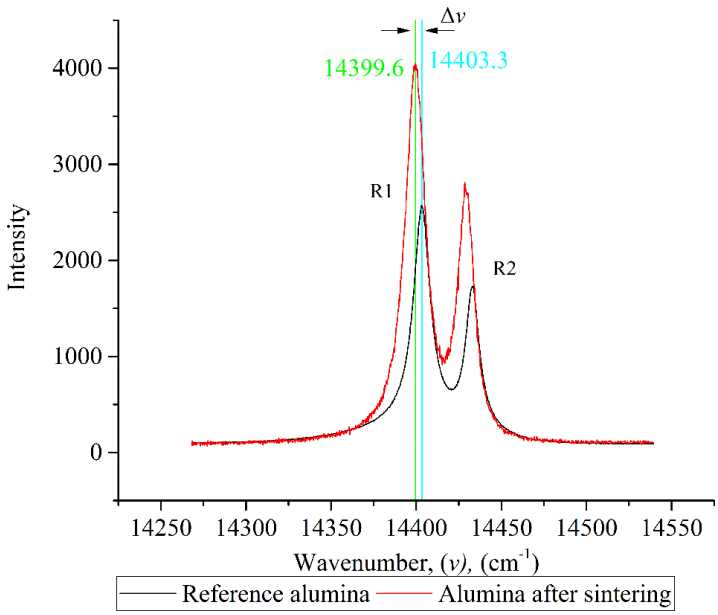

Figure 3. Representative fluorescence spectrum from a cell with a thickness ratio: 40:1:2, A:E:C and the shift (Δv) from reference spectrum after sintering.

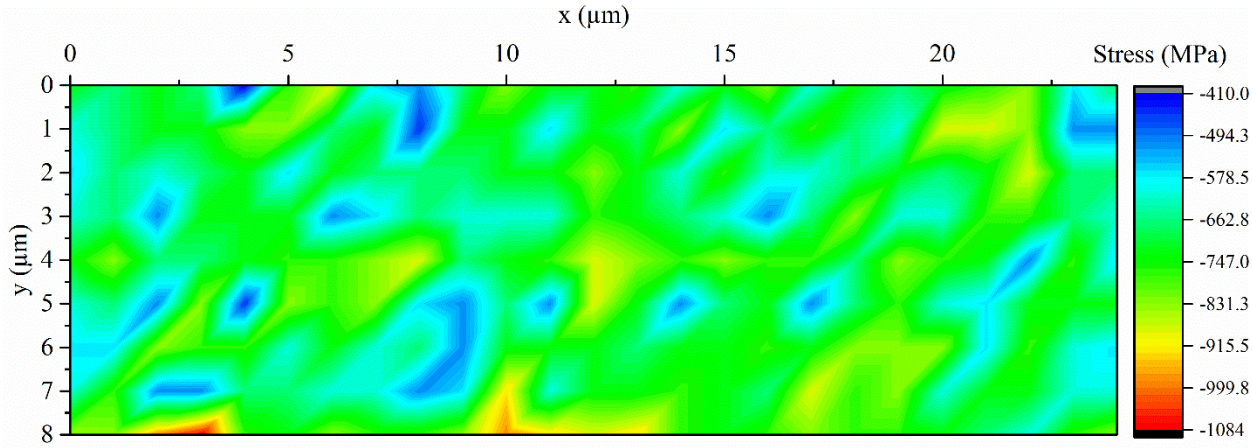

Figure 4. Residual stress results of cell from Fluorescence spectroscopy.

Table 3. Mean stress measurement along y direction on alumina sintered with SC-SOFC

Mean stress measurement along y direction on alumina sintered with SC-SOFC (MPa)									
	X direction	0	1	2	3	4	5	6	7
Cell		-651.182	-703.883	-675.337	-739.017	-675.337	-721.45	-721.45	-686.316
	X direction continue	8	9	10	11	12	13	14	15
Cell		-633.615	-640.203	-769.759	-686.316	-796.11	-752.192	-695.1	-706.079
	X direction continue	16	17	18	19	20	21	22	23
Cell		-701.687	-708.275	-732.429	-736.821	-714.863	-712.667	-739.017	-655.574
	X direction continue	24							
Cell		-640.203							

The total average residual stress on the alumina particles located between the cell's electrolyte and cathode was measured to be -703.795 MPa at room temperature utilizing fluorescence spectroscopy. The overall average residual stress includes sintering stress during sintering and co-efficient of thermal expansion mismatch stress during cooling. The estimated residual stresses in the cell's cathode layer because of CTE mismatch during cooling was calculated as -324 MPa. Likewise, the estimated residual stresses in the single composite new layer was found to be 15.96 MPa from calculation. These results show that the dominant factor of the total mean residual stress is the stress developed during sintering (-395.755 MPa) owing to different shrinkage behavior of layers as the stress due to CTE misfit is low compared to residual stress arisen during sintering.

4. Conclusions

The fluorescence spectroscopy technique was applied to measure the total residual stress between electrolyte and cathode of a cell after sintering at room temperature. The residual stress in the cathode and electrolyte layer of the cell because of CTE misfit during cooling was also obtained from the analytical equations. According to results a high total residual stress of -703.795 MPa measured between the electrolyte and cathode of the cell after sintering. The stress developed during sintering (sintering stress=-395.755 MPa) due to different shrinkage behavior of adjacent layers is the main contribution of this residual stress compared to stress developed during cooling because of CTE mismatch.

Acknowledgment

The work was supported by the Turkish Ministry of Higher Education and the EPSRC's the India-UK Collaborative Research Initiative in Fuel Cells project on "Modelling Accelerated Ageing and Degradation of Solid Oxide Fuel Cells" (EP/I037059/1), and also the EPSRC's UK-Korea Collaborative Research Activity in Fuel Cells project on "Novel diagnostic tools and techniques for monitoring and control of SOFC stacks" (EP/M02346X/1).

Conflict of Interest Statement

There is no conflict of interest between the authors.

Contributions of the authors

All contributions to this study belong to the authors.

Statement of Research and Publication Ethics

The study is complied with research and publication ethics

References

[1] G. De Portu, L. Micele, Y. Sekiguchi, and G. Pezzotti, "Measurement of residual stress distributions in Al_2O_3 / 3Y-TZP multilayered composites by fluorescence and raman microprobe piezo-spectroscopy," Acta Mater., vol. 53, no. 5, pp. 1511–1520, 2005.

[2] P. Z. Cai, D. J. Green, and G. L. Messing, "Constrained densification of alumina/zirconia hybrid laminates, II: viscoelastic stress computation," J. Am. Ceram. Soc., vol. 48, no. 8, pp. 1940–1948, 1997.

[3] H. Z. Wu, S. G. Roberts, and B. Derby, "Residual stress distributions around indentations and scratches in polycrystalline Al_2O_3 and Al_2O_3 / SiC nanocomposites measured using fluorescence probes," Acta Mater., vol. 56, no. 1, pp. 140–149, 2008.

[4] B. C. Feldmann, T. Jüstel, C. R. Ronda, and P. J. Schmidt, "Inorganic luminescent materials : 100 years of research and application," Adv. Funct. Mater., vol. 13, no. 7, pp. 511–516, 2003.

[5] A. Edgar, "Luminescent," in Springer Handbook of electronic and photonic materials, 2nd Editio., S. Kasap and P. Capper, Eds. Springer, 2017, pp. 997–1012.

[6] J. He and D. R. Clarke, "Determination of the Piezospectroscopy coefficients for chromium-doped sapphire," J. Am. Ceram. Soc., vol. 78, no. 5, pp. 1347–1353, 1995.

[7] L. Grabner, "Spectroscopic technique for the measurement of residual stress in sintered Al_2O_3," J. Appl. Physic, vol. 580, no. 1978, pp. 1–5, 1996.

[8] D. Di Marco et al., "Dielectric properties of pure alumina from 8 GHz to 73 GHz," J. Eur. Ceram. Soc., vol. 36, no. 14, pp. 3355–3361, 2016.

[9] P. Auerkari, "Mechanical and physical properties of engineering alumina ceramics," Espoo, 1996.

[10] H. N. Kim, H. J. Park, and G. M. Choi, "The effect of alumina addition on the electrical conductivity of

Gd-doped ceria," J. Electroceramics, vol. 17, no. 2–4, pp. 793–7982, 2006.
[11] R. Chockalingam, S. Chockalingam, and V. R. W. Amarakoon, "The electrical properties of microwave sintered gadolinia doped ceria – alumina nano-composite electrolyte," J. Power Sources, vol. 196, no. 4, pp. 1808–1817, 2011.
[12] J. Lee, K. Choi, B. Ryu, B. Shin, and I. Kim, "Effects of alumina additions on sintering behavior of gadolinia-doped ceria," Ceram. Int., vol. 30, no. 5, pp. 807–812, 2004.
[13] S. Huang, J. G. P. Binner, B. Vaidhyanathan, and R. I. Todd, "Quantitative analysis of the residual stress and dislocation density distributions around indentations in alumina and zirconia toughened alumina (ZTA) ceramics," J. Eur. Ceram. Soc., vol. 34, no. 3, pp. 753–763, 2014.
[14] G. A. Myers, C. A. Michaels, and R. F. Cook, "Quantitative mapping of stress heterogeneity in polycrystalline alumina using hyperspectral fl uorescence microscopy," Acta Mater., vol. 106, pp. 272–282, 2016.
[15] C. A. Michaels and R. F. Cook, "Determination of residual stress distributions in polycrystalline alumina using fl uorescence microscopy," Mater. Des., vol. 107, pp. 478–490, 2016.
[16] M. Materials, S. Centre, and G. Street, "Fragmentation in alumina fibre reinforced epoxy model composites monitored using fluorescence spectroscopy," J. Mater. Sci., vol. 31, no. 13, pp. 3349–3359, 1996.
[17] Q. Ma and D. R. Clarke, "Stress measurement in single-crystal and polycrystalline ceramics using their optical fluorescence," J. Am. Ceram. Soc., vol. 76, no. 6, pp. 1433–1440, 1993.
[18] R. . Todd, A. R. Boccaccini, R. Sinclair, R. B. Yallee, and R. J. Young, "Thermal residual stresses and their toughening effect in Al_2O_3 platelet reinforced glass," Acta Mater., vol. 47, no. 11, pp. 3233–3240, 1999.
[19] E. Feher and M. D. Sturge, "Effect of stress on the trigonal splittings of d3 ions in sapphire (a-Al_2O_3)," Phys. Rev., vol. 172, no. 2, pp. 243–249, 1968.
[20] J. He, I. . Beyerlein, and D. . Clarke, "Load transfer from broken fibers in continuous fiber Al_2O_3-Al composites and dependence on local volume fraction," J. Mech. Phys. Solids, vol. 47, pp. 465–502, 1999.
[21] R. G. Munro, G. J. Piermarini, and S. Block, "Model line shape analysis for the ruby R lines used for pressure measurement," J. Appl. Physic, vol. 57, no. 2, pp. 165–169, 1985.
[22] D. D. Ragan, D. R. Clarke, and D. Schiferl, "Silicone fluid as a high-pressure medium in diamond anvil cells," Am. Inst. Physic, vol. 2, no. 1996, pp. 494–496, 67AD.
[23] Y. Sayan, V. Venkatesan, E. Guk, H. Wu, and J. S. Kim, "Single-step fabrication of an anode supported planar single-chamber solid oxide fuel cell," Int. J. Appl. Ceram. Technol., no. April, pp. 1–13, 2018.
[24] A. Atkinson and A. Selçuk, "Residual stress and fracture of laminated ceramic membranes," Acta Mater., vol. 47, no. 3, pp. 867–874, 1999.
[25] A. Selçuk and A. Atkinson, "Elastic properties of ceramic oxides used in solid oxide fuel cells (SOFC)," J. Eur. Ceram. Soc., vol. 17, no. 12, pp. 1523–1532, 1997.
[26] "Maryland Tape Casting." [Online]. Available: http://www.marylandtapecasting.com/.
[27] S. C. Singhal and K. Kendall, High temperature solid oxide fuel cells:fundementals, design and applications. Oxford: Elsevier Advanced Technology, 2003.
[28] S. Bandopadhyay, "Evaluation of elastic properties of reduced NiO-8YSZ anode- supported bi-layer SOFC structures at elevated temperatures in ambient air and reducing environments," J. Mater. Sci. Lett., no. July, pp. 778–785, 2009.
[29] K. Raju, S. Kim, J. H. Yu, S. H. Kim, Y. H. Seong, and I. S. Han, "Rietveld refinement and estimation of residual stress in GDC-LSCF oxygen transport membrane ceramic composites," Ceram. Int., vol. 44, no. February, pp. 10293–10298, 2018.
[30] Y. Chou, J. W. Stevenson, T. R. Armstrong, and L. R. Pederson, "Mechanical properties of LSCF mixed-conducting perovskites made by the combustion synthesis technique," J. Am. Ceram. Soc., vol. 83, pp. 1457–1464, 2000.